Multiwalled Carbon Nanotube (MWCNT) Reinforced Cellulose Fibers by Electrospinning

Ping Lu and You-Lo Hsieh*

Fiber and Polymer Science, University of California, Davis, California 95616

ABSTRACT Multiwalled carbon nanotubes (MWCNTs) were successfully incorporated in ultrafine cellulose fibers by electrospinning MWCNT-loaded cellulose acetate (CA) solutions, followed by deacetylation of CA to cellulose (cell). The mean fiber diameter reduced from 321 nm of the as-spun fibers to 257 and 228 nm of those with 0.11 and 0.55 wt % MWCNTs, respectively, and became more uniform. Hydrolysis of CA to cell further reduced the mean fiber sizes by another 8−16%. The MWCNTs were observed to be well-aligned along the fiber axes. The MWCNT/cell composite fibers had increased specific surface, from 4.27 m^2/g to 5.07 and 7.69 m^2/g at 0.11 and 0.55 wt % MWCNTs, respectively, and much improved water wettability. The mechanical properties of the fibers were also greatly enhanced with increased MWCNT loading levels. The fact that MWCNTs were observed in only about a third of the fibers at a very low 0.55 wt % loading suggests significantly higher tensile strength may be achieved by a further increase in MWCNT loadings.

KEYWORDS: carbon nanotube • cellulose • electrospinning • reinforcement • tensile strength

INTRODUCTION

Since their discovery by Ijima in 1991 (1), multiwalled carbon nanotubes (MWCNTs) have attracted intensive attention because of their extraordinary mechanical, electrical, thermal, chemical, and structural properties on the microscopic scale (2). To bridge the dimensional and property gap between MWCNTs and engineering materials, researchers have devoted tremendous efforts to translate the superior properties of MWCNTs to macroscale structures for technological applications (3, 4). With the combination of low density, high aspect ratio, high stiffness, and extremely high strength, MWCNTs stand out as the ultimate reinforcing nanofillers for the construction of high-performance polymer composites (5, 6).

Among the various methods, electrospinning has shown promise for fabricating MWCNTs reinforced polymer fibers (7, 8). Electrospinning is a simple and yet versatile technique for generating continuous one-dimensional fibers from polymer solutions or melts, driven by a high-voltage electric charge (9). This process produces fibers with diameters from several micrometers down to tens of nanometers, and thus provides an ideal route to bridge the dimensional gap between the nano and macro worlds (10). The electrospun fibrous materials possess a variety of interesting characteristics such as large specific surface area, wide ranging porosity, and excellent flexibility (11). The electrospun fibers, however, are not as strong because of the lower chain orientation (12) resulting from the low stretching forces in the spinning process (13). Incorporation of both single-walled carbon nanotubes (SWCNTs) and MWCNTs with polyacrylonitrile (PAN) has shown to improve the mechanical properties of the electrospun fibers (14, 15). Furthermore, it was shown that most of the embedded MWCNTs were aligned along the fiber axes (16).

Majority of MWCNT−polymer composite fibers are generated from the mixtures of MWCNTs with synthetic polymers such as PAN (12), poly(vinylidene difluoride) (PVDF) (17), polystyrene (PS) (18), poly(ethylene oxide) (PEO) (19), poly(lactic acid) (PLA) (20), polycarbonate (PC) (21), polyurethane (PU) (22), poly(methyl methacrylate) (PMMA) (23) and nylon (24) because of the easy dispersion of MWCNTs in the solvents like dimethylformamide (DMF) or water for these polymers. The reinforcing effects of MWCNTs to natural biopolymers such as cellulose, lignin, chitosan, and protein in fiber form were rarely addressed in the published literature (25, 26), mainly because of the difficulties in dispersing MWCNTs in the solvents for the biopolymers.

The objective of this work is to fabricate cellulose nanocomposites reinforced with MWCNTs by electrospinning method. Cellulose, the most abundant natural resource on earth, is known for its excellent biocompatibility and biodegradability as well as its thermal and mechanical properties (27). Electrospinning cellulose from direct solvents such as *N*-methylmorpholine oxide/water (NMMO/H_2O) (28), lithium chloride/*N*,*N*-dimethyl acetamide (LiCl/DMAc) (29), and more recently developed ionic liquids (30) and ethylene diamine/potassium thiocyanate (ED/KSCN) (31) has been reported. However, these solvents or the associated salts are not completely volatile and additional coagulation steps are required for their complete removal (32) to avoid solvent-induced deformation or loss of the fiber morphology (33).

* To whom correspondence should be addressed. Tel.: (530) 752 0843. E-mail: ylhsieh@ucdavis.edu.
Received for review May 11, 2010 and accepted July 19, 2010

DOI: 10.1021/am1004128

Furthermore, direct electrospinning of cellulose has shown to produce high irregularity across the sheets (30) that is due to polymer jet instability in the electrospinning process. Alternatively, cellulose fibers have also been obtained from electrospinning of its derivatives, such as cellulose acetate (CA) (34), hydroxypropyl cellulose (HPC) (35), and hydroxypropylmethyl cellulose (36), then regenerate the cellulose. CA, because of its ready solubility in common solvents, has remained to be the most common cellulose derivative for electrospinning (37, 38).

We have successfully produced pure cellulose fibers from electrospinning CA in acetone/dimethylacetamide (DMAc) mixtures of varying ratios, followed by deacetylation in aqueous sodium hydroxide (NaOH) solution (38). This process in preparing pure cellulose fibrous membranes was robust and proficient in producing uniform fibers whose sizes and packing could be easily tuned by varying the solution properties and electrospinning conditions. The acid-treated MWCNTs are readily soluble in DMAc, and thus can be loaded in the mixed acetone/DMAc solvent system. To proof the concept of fabricating MWCNT-loaded cellulose fibers, the MWCNT loading was approached at low levels in this study. The goal was to study the fiber morphology, the pore and surface structures and the mechanical properties of the MWCNT−cellulose composite fibers.

EXPERIMENTAL SECTION

Materials. Cellulose acetate (CA) (39.8 wt % acetyl content, average $M_n \sim 30\,000$ Da) was purchased from Sigma-Aldrich Chemical Co. Inc. (Milwaukee, WI). Acetone and *N*,*N*-dimethylacetamide (DMAc), from EMD Chemicals, were used as-received without further purification. Multiwalled carbon nanotubes referred to as MWCNTs (purity >95%; outside diameter, 10−30 nm; inside diameter, 5−10 nm; length, 5−15 μm) were obtained from Nanostructured & Amorphous Materials Inc. The as-received MWCNTs were first refluxed in a 6 M HNO_3 solution for 12 h at a 400:1 acid:MWCNT w/w ratio to remove the impurities from the MWCNT surfaces, followed by washing in water until reaching neutral pH. After drying, the surface-oxidized MWCNTs were well-dispersed in DMAc under stirring and sonicating for 45 min, which was used as the stocking solution for electrospinning. All water used was purified by Milli-Q plus water purification system (Millipore Corporate, Billerica, MA).

Electrospinning of Composite Fibers. The cellulose and MWCNT/cellulose (MWCNT/cell) fibrous sheets were fabricated by electrospinning 15 wt % CA in 2:1 w:w acetone/DMAc and with MWCNTs at two loading levels, followed by alkaline hydrolysis to convert CA to cellulose. The MWCNT/CA solutions were prepared at 0.01/15 and 0.05/15 ratios. On the basis of the 39.8 wt % acetyl content in the CA used, the MWCNT loadings in the final MWCNT/cell composites regenerated from 0.01/15 and 0.55 wt % MWCNT/CA were calculated to be 0.11 and 0.55 wt %, respectively (Herein refer to 0.11 and 0.55 wt % MWCNT/cell). Each solution was loaded into a 20 mL syringe (National Scientific) fitted with a 23 gauge flat metal needle (BD Medical Franklin Lakes, NJ) and fed at 1 mL/h with a syringe pump (KDS 200, KD Scientific, USA). The MWCNT/CA mixtures were electrospun by applying a 14.25 kV voltage using a DC power supply (ES 30−0.1 P, Gamma High Voltage Research Inc., Ormond Beach, FL) to a horizontally positioned metal needle at 27 °C and 34% relative humidity. The charged jet sprayed into fine fibers that were collected on a vertical aluminum plate (30 cm × 30 cm) placed 25 cm from the tip of the needle. The electrospun MWCNT/CA fibrous sheets were deacetylated in 0.05 M aqueous NaOH solution at ambient temperature for 7 days to regenerate into cellulose. The fibrous MWCNT/cell sheets were then rinsed with water until neutral and kept over ion-exchange resin (Rexyn I-300 H−OH from Fisher Scientific, Inc.) for 10 days to remove the residue metal ions. The samples were thoroughly washed by water and then vacuum-dried at ambient temperature for 48 h. For comparison, pure cell fibrous sheet was also produced by electrospinning 15 wt % CA solution using the above setup and deacetylation procedures.

Characterization. The microstructures and the surface morphologies of the products were examined by a field-emission scanning electron microscope (SEM) (XL 30-SFEG, FEI/Philips, USA) after 2 min gold coating (Bio-Rad SEM coating system). The fiber diameter and size distribution of the samples were evaluated from at least 100 representative fibers of the samples by an image analyzer (analySIS FIVE, Soft Imaging System). Raman spectra were recorded from 200 to 2000 cm^{-1} using the Argon 514 nm laser in 2D mode by a Renishaw RM1000 spectrophotometer coupled with a Leica CCD detector. The crystalline phases present in the powder samples were determined by X-ray diffraction (XRD) (Scintag XDS 2000 powder diffractometer) at 45 kV and 40 mA from 5° to 80° with a Ni-filtered Cu K a_1 radiation ($\lambda = 1.542$ Å). The Fourier transform infrared (FTIR) spectra were collected from 4000 to 400 cm^{-1} at 128 scans with a 4 cm^{-1} resolution on a Nicolet 6700 spectrometer (Thermo Fisher Scientific, USA). The surface area, pore volume and pore size distribution of cell and MWCNT/cell were derived from N_2 adsorption−desorption isotherms at 77 K with the Brunauer−Emmett−Teller (BET) equation in a $p/p° = 0.06-0.20$ relative pressure range and the Barrett−Joyner−Halenda (BJH) method from the adsorption branch of the isotherms using a surface area and porosity analyzer (ASAP 2020, Micromeritics, USA). The dynamic wetting and absorption of samples (5 mm × 25.4 mm) in water were measured by a tensiometer (K14, KRÜSS, USA) and the equilibrium wetting force and water absorption were derived by a method reported previously (39). The tensile properties of the cell and MWCNT/cell fibrous sheets were determined by a tensile tester (Instron 5566, Illinois Tool Works Inc., USA) at a 10 mm gauge length and a 5 mm/min cross-head speed at 21 °C and 65% relative humidity. The specimens were cut along the vertical direction of the electrospun fibrous membranes to a 5 mm wide and 20 mm length size. The thickness and weight of each fibrous membrane were measured by a thickness tester (Custom Scientific Instruments, Inc., Whippany, NJ) and a balance with accuracy to 0.01 mg (AUW220D, Shimadzu), respectively. For each fibrous mat, ten samples within similar (±10%) thickness (~0.1 mm) and weight (~2 mg) or an apparent density (~0.2 mg/mm^3) were used for tensile measurements. The Young's modulus of the samples is derived from the slope of the initial linear part of the stress−strain curves.

RESULTS AND DISCUSSION

The as-spun CA and MWCNT filled CA as well as alkaline hydrolyzed counterparts were characterized by FTIR and XRD. In all three hydrolyzed samples, the strong CA acetyl carbonyl adsorption at 1746 cm^{-1} disappeared, along with the appearance of a much broader and stronger hydroxyl (OH) peak at around 3400 cm^{-1}, CH stretching at 2900 cm^{-1}, OH bending of adsorbed water at 1646 cm^{-1}, HCH and OCH in-plane bending at 1418 cm^{-1}, CH deformation at 1372 cm^{-1}, and COC, CCO, and CCH deformation and stretching at 896 cm^{-1} (40), indicating clearly full deacetylation of CA and full regeneration of cell (Figure 1). Furthermore, the XRD patterns (Figure 2) of the three deacetylated samples showed three cellulose characteristic peaks cen-

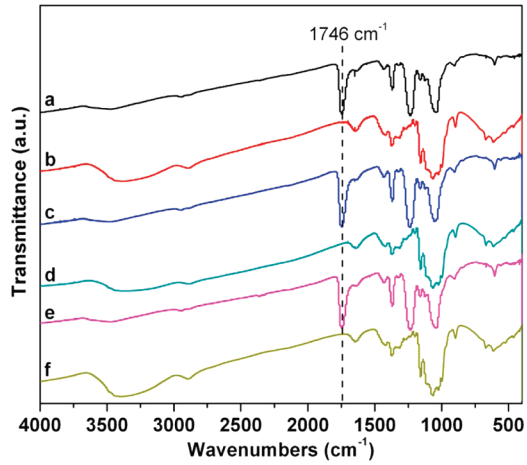

FIGURE 1. FTIR spectra of (a) as-spun CA, (b) cell, (c) as-spun 0.11 wt % MWCNT/CA, (d) 0.11 wt % MWCNT/cell, (e) as-spun 0.55 wt % MWCNT/CA, and (f) 0.55 wt % MWCNT/cell.

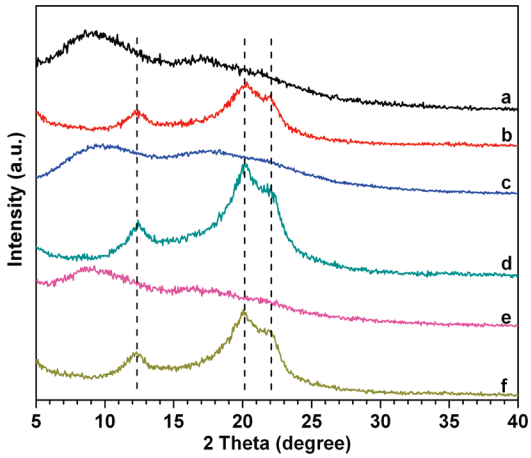

FIGURE 2. XRD patterns of (a) as-spun CA, (b) cell, (c) as-spun 0.11 wt % MWCNT/CA, (d) 0.11 wt % MWCNT/cell, (e) as-spun 0.55 wt % MWCNT/CA, and (f) 0.55 wt % MWCNT/cell from e.

tered at $2\theta = 12.3$, 20.2, and 22.0° (curves b, d, and f), whereas those of as-spun samples had two broad amorphous halos in the ranges of 8.5−11.0° and 14.1−20.2° (curves a, c, and e). The XRD results together with the FTIR data confirmed that the CA was successfully transformed to cell by deacetylation in the aqueous NaOH solution. For the hydrolyzed fibers, the 20.2° peak is close to the typical 101 reflection of cellulose II ($2\theta = 19.8°$), whereas the one at 22.0° is close to the 002 reflection of cellulose I ($2\theta = 22.5°$). However, both are far weaker than those of cellulose I in cotton (41) and cellulose II in regenerated cellulose (42). These XRD patterns suggest that low quantities of cellulose I and II crystalline allomorphs may be present in the fully hydrolyzed cell fibers and the presence of MWCNTs appears to slightly enhance the crystallinity. However, the typical XRD peak of MWCNTs at around 26° was not seen in the spectra. The absence of MWCNT characteristic peak in XRD is thought to be mainly due to the very low MWCNT contents in the fibers.

The cell, 0.11 wt % MWCNT/cell, and 0.55 wt % MWCNT/cell sheets appear similarly uniform in texture. The regenerated cell sheet is white as expected from pure cellulose, as in cotton or cellulose filter paper (Figure 3a). The 0.11 wt %

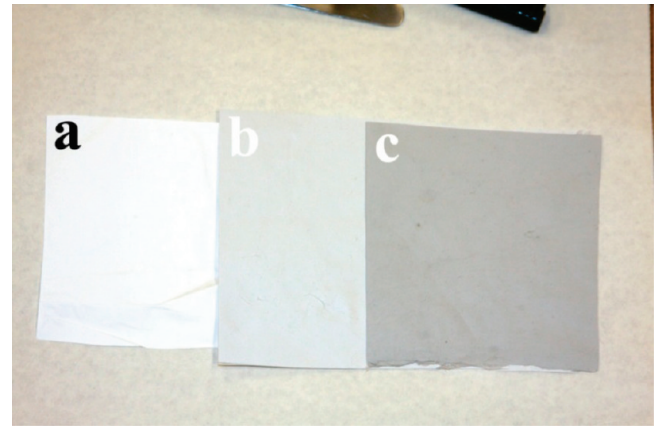

FIGURE 3. Optical images of electrospun fiber sheets of (a) cell, (b) 0.11 wt % MWCNT/cell, and (c) 0.55 wt % MWCNT/cell.

MWCNT/cell was light ash gray (Figure 3b) and darkened to gray at 0.55 wt % of MWCNTs (Figure 3c). The dark color appeared homogeneously on the entire MWCNT/Cell fibrous composite sheets, indicating even distribution of MWCNTs at the macroscopic level. Acid pretreatment has been shown to introduce carboxylic acid groups as well as hydroxyl groups onto the MWCNT surfaces (12, 16, 19), enabling its dispersion in aprotic polar solvents such as DMAc used in this study (6). It is thought that the newly introduced carboxylic groups caused the negatively charged MWCNTs to not only repel from each other but also attract the positively charged amide groups of DMAc via the strong columbic interaction.

The SEMs of the as-spun fibrous membranes showed slightly decreasing fiber sizes with increasing MWCNTs, likely ascribed to the enhanced electric conductivity of the solutions by the MWCNTs (Figure 4). Deacetylation also reduced the average fiber diameters from 321 nm for CA to 267 nm for cell counterpart as well as for the MWCNT loaded from 257 to 237 nm and from 228 to 193 nm at 0.11 and 0.55 wt %, respectively. The fibers also became more uniform in sizes with deacetylation, as shown by the decreased standard deviation from 258 to 90 nm, 113 to 71 nm, and 99 to 73 nm for unloaded and MWCNT-loaded at 0.11 and 0.55 wt %, respectively (Figure 5). The as-spun CA and MWCNT/CA composite fibers as well as their corresponding regenerated cell and MWCNT/cell fibers show denser fiber packing in all the three regenerated samples. This is a result of increasing attraction among cellulose fibers through hydrogen-bond formation from water evaporation in the drying process.

High-resolution SEM images, shown in Figure 6, further revealed the surface roughness induced by the deacetylation process. Because any residual NaOH or sodium salts had been removed by extensive water washing until pH neutral and prolonged ion exchange, the newly observed rough fiber surfaces show that replacing the acetyl with hydroxyl groups during deacetylation of CA in mild NaOH generate porosity on the fiber surfaces not noticed in our previous studies (38, 40). Moreover, no protrusion of MWCNTs as well as no free MWCNTs was observed in the MWCNT/cell 3D fibrous

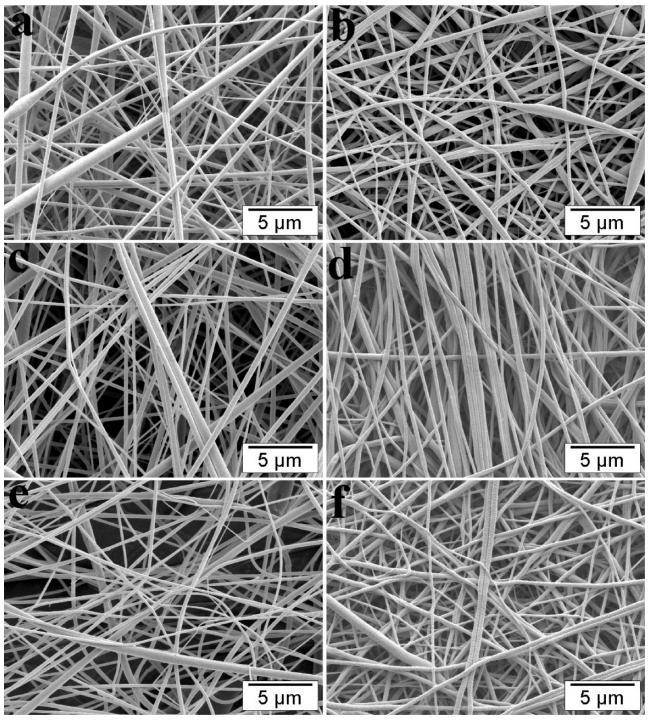

FIGURE 4. SEM images of (a) as-spun CA, (b) cell, (c) as-spun 0.11 wt % MWCNT/CA, (d) 0.11 wt % MWCNT/cell, (e) as-spun 0.55 wt % MWCNT/CA, and (f) 0.55 wt % MWCNT/cell.

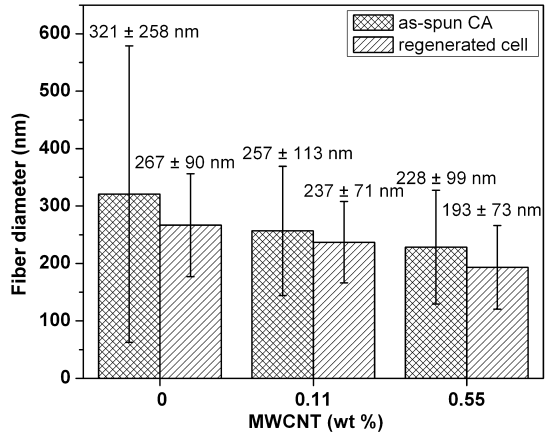

FIGURE 5. Size distributions of as-spun and regenerated fibers.

structure (Figure 6b,c), indicating the successful inclusion of MWCNTs in cell fiber matrix.

The presence of MWCNTs in cell fibrous sheets was confirmed by Raman spectroscopy (Figure 7). The Raman spectrum of pure cell is featureless in the range of 200−2000

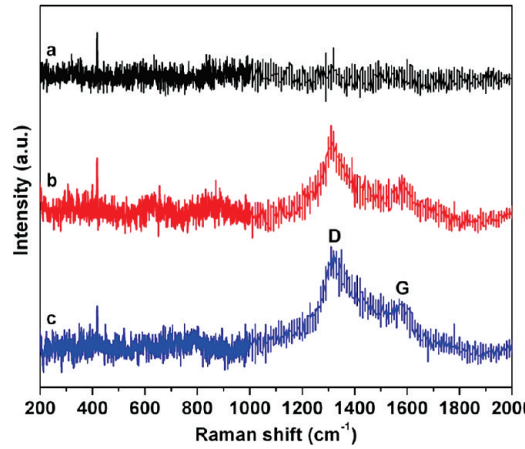

FIGURE 7. Raman spectra of: (a) cell, (b) 0.11 wt % MWCNT/cell, and (c) 0.55 wt % MWCNT/cell.

cm^{-1}, whereas MWCNT/cell composites at both 0.11 and 0.55 wt % MWCNT loading levels showed strong Raman scattering with two characteristic peaks of MWCNTs centered at 1320 (D band) and 1590 (G band) cm^{-1} that had been assigned to the disordered and ordered lattices of graphite crystals, respectively (12, 26). The intensity of these two Raman scattering peaks increased with increasing MWCNT contents in MWCNT/cell composites, but not in proportion to the exact quantity of MWCNTs (3).

The distribution and orientation of the MWCNTs in the as-prepared MWCNT/cell composite fibers were further examined by TEM. With higher electron density (12), the MWCNTs appeared as dark tubular structures and in isolation among the matrix polymer without any sign of agglomeration (Figure 8). Most MWCNTs are well-aligned along the fiber axis. This orientation of MWCNTs is very likely to be associated with the extreme high shear and elongation forces along the axis of liquid jet from spraying and whipping instability in electrospinning, leading to the disentanglement and stretching of the MWCNTs (43). The well oriented MWCNTs were then quickly fixed inside the fibers upon fast evaporation of solvent (Figure 8c,d) (44). However, the MWCNTs were only observed in about a third of the 0.55 wt % loaded and around one-tenth of the 0.11 wt % loaded fibers. These observations indicate that considerably higher MWCNT contents are necessary to distribute continuously along the lengths of the fibers.

Fracturing the MWCNT/cell composite fibers under liquid nitrogen showed some protruding MWCNTs out of the broken cross sections, as shown by circles in Figure 9, demonstrating the pullout effect of the MWCNTs in cell

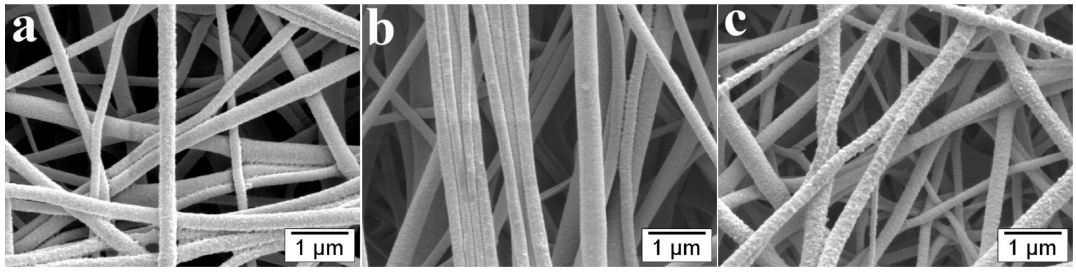

FIGURE 6. SEM images showing the surface morphologies: (a) cell, (b) 0.11 wt % MWCNT/cell, and (c) 0.55 wt % MWCNT/cell fibers.

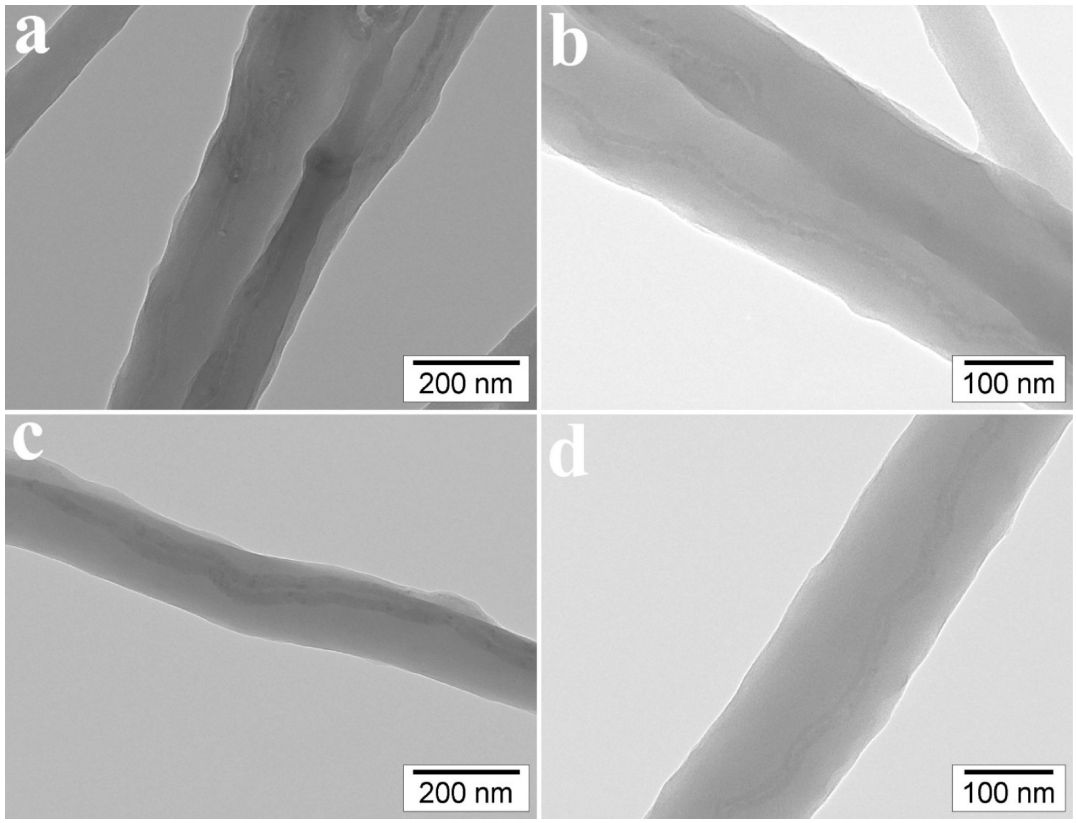

FIGURE 8. TEM images showing the embedded MWCNTs oriented along the axes of 0.55 wt % MWCNT/cell fibers.

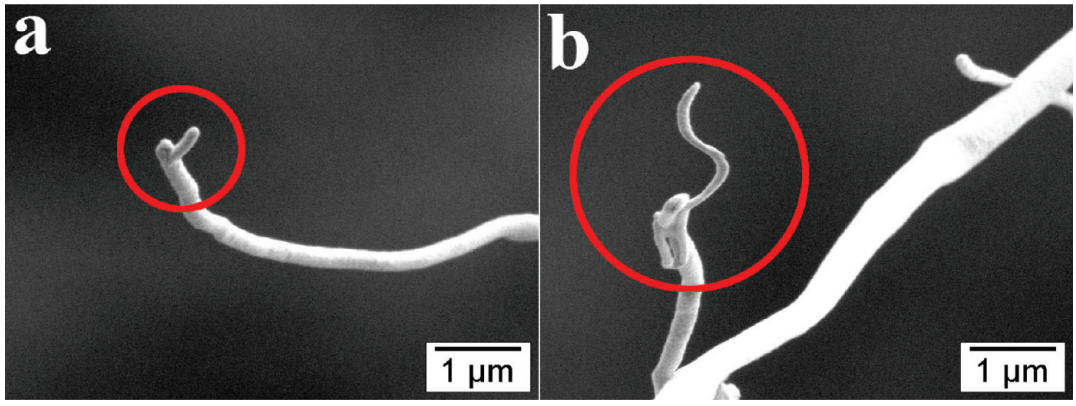

FIGURE 9. SEM images showing the pullout effect of the embedded MWCNTs at the broken cross section of 0.55 wt % MWCNT/cell fibers by applying tensile force under liquid nitrogen freezing.

matrix under tensile force, similar to the report on MWCNT/PC composite fibers (21). However, not every fracture cross section showed exposed MWCNTs, a sign that MWCNTs were not distributed in a continuous manner along the lengths of the fibers, again consistent with TEM observation (Figure 8).

The surface areas and porosities of the as-prepared cell and two MWCNT/cell fibers were measured by nitrogen adsorption–desorption method at 77 K (Figure 10A). All three samples exhibited type II isotherms with nearly reversible loops, indicating their nonporous or macroporous nature. The type II isotherm is also characterized by unrestricted monolayer–multilayer adsorption at high $p/p°$ as seen in Figure 10A. The macroporous nature was confirmed by the pore size distribution calculated from the adsorption branch of the isotherms by Barrett–Joyner–Halenda (BJH) method (Figure 10B). The pore size distributions were wide in all three cases, ranging from 10 to 200 nm. Moreover, the calculated cumulative pore volumes are very close among the three, which are 0.02, 0.02, and 0.03 cm^3/g for cell, 0.11, and 0.55 wt % MWCNT/cell, respectively. The low cumulative pore volumes disclosed that the embedded MWCNTs were surrounded by cell chains in the matrix, leaving no interfacial free spaces between MWCNTs and the polymer matrix. This suggests the strong interfacial interactions between MWCNTs and cell matrix. However, the Brunauer–Emmett–Teller (BET) surface area of cell increased with the increasing of MWCNT contents, i.e., from 4.27 to 5.07 and 7.69 m^2/g at 0.11 and 0.55 wt % loadings, respectively. Considering the nearly unchanged density as

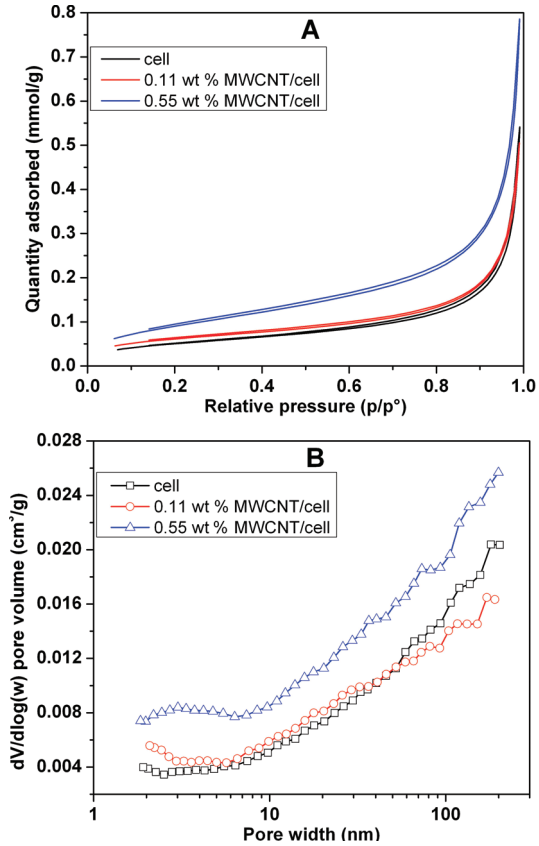

FIGURE 10. Pore characteristics of cell and MWCNT/cell: (A) Nitrogen adsorption−desorption isotherms at 77 K, (B) pore size distribution calculated from the adsorption branch of the isotherms by BJH method.

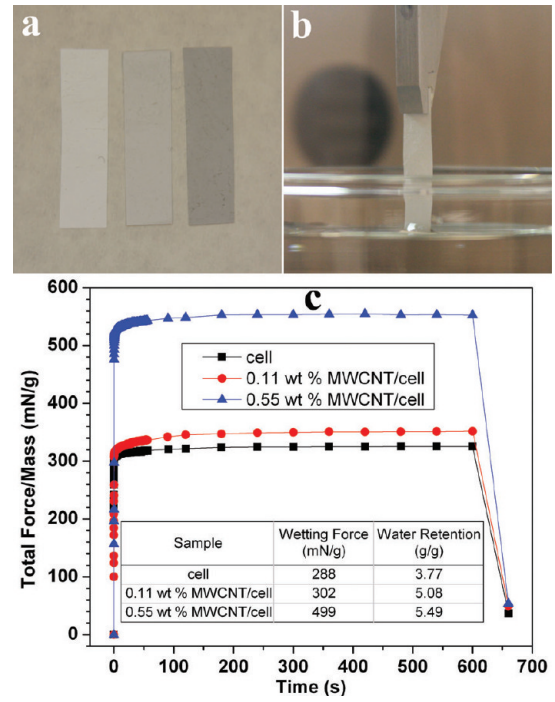

FIGURE 11. Dynamic water wetting and absorption curves of as-prepared fibrous sheets: (a) 5 mm wide and 25.4 mm long samples, (b) lower edge in contact with water, (c) wetting force profile from initial water contact to equilibrium water wetting and saturation at ~120 s and final pull out at 660 s.

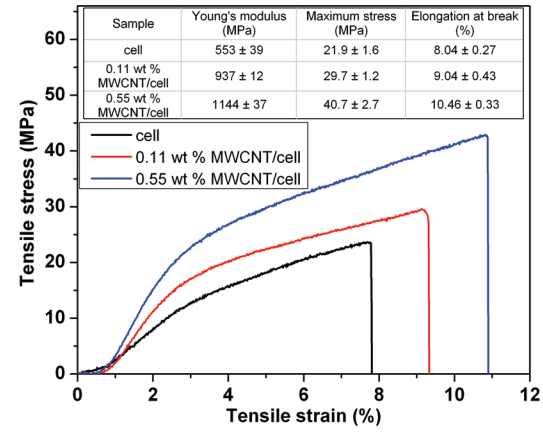

FIGURE 12. Mechanical properties of cell, and 0.11 and 0.55 wt % MWCNT/cell fibrous sheets. At least 10 samples were tested for each material and the stress−strain curves shown here are representative of each.

well as pore volume from the very small amount of MWCNTs (less than 0.6% of the entire mass), the increased specific surface for the MWCNT/cell fibers may be attributed to a combination of increasing internal surfaces of MWCNTs and the smaller fiber diameters resulting from increased MWCNT contents observed before (Figure 5).

For dynamic wetting and absorption in water, each sample at 5 mm width and 25.4 mm length (Figure 11a) was brought into contact with water at the lower edge (Figure 11b) and the simultaneous wetting force and absorption were measured by a tensiometer. Upon reaching the equilibrium, the sample was lifted off the water surface to record the water absorbed. The dynamic water wetting and absorption profiles of all three samples demonstrated super water wetting and absorption within seconds, reaching 97% equilibrium in <90 s (Figure 11). Compared with cell, the 0.11 wt % MWCNT/cell showed a small increase in wetting force, from 288 to 302 mN/g, indicating slightly improved hydrophilicity. The 0.55 wt % MWCNT/cell fibrous sheet, on the other hand, exhibited a vastly increased wetting force of 499 mN/g, significantly more hydrophilic. The enhanced wetting, particularly from 0.11 to 0.55 wt % loading, is attributed to the hydrolysis-induced increased surface roughness observed earlier (Figure 6b,c). Water absorption was also increased with the inclusion and higher quantity of MWCNTs, i.e., from 3.77 g of water per g of cell to 5.08 and 5.49 g/g of those loaded with 0.11 and 0.55 wt % MWCNTs. Water absorption in fibrous materials is governed by fiber surface wetting behavior and the interfiber pore volume. The water absorption of the MWCNT loaded fibrous sheets reflect their similar interfiber pore structure, but more improved wetting of the higher MWCNT loaded sample.

Typical stress−strain curves with calculated values of the three samples are presented in Figure 12. The cell fibrous sheets exhibited exceptional Young's modulus of 553 MPa and tensile strength of 21.9 MPa but relatively low elongation at break of 8.04%. With MWCNTs, the tensile strength and modulus were significantly improved and the elongation slightly increased. The Young's modulus was increased to 937 and 1144 MPa at 0.11 and 0.55 wt % MWCNT, while the tensile strength also increased to 29.7 and 40.7 MPa,

Table 1. BET Surface Areas and Pore Volumes of the Samples

	cell	0.11 wt % MWCNT/cell	0.55 wt % MWCNT/cell
BET surface area (m^2/g)	4.27	5.07	7.69
pore volume (cm^3/g)[a]	0.02	0.02	0.03

[a] Between 1.7 and 300 nm and from adsorption branch of the isotherms calculated by BJH method.

respectively. It is remarkable that both the tensile strength and modulus doubled at a relatively low 0.55% MWCNT content. The increase in the modulus, tensile strength and elongation could be attributed to the effective load transfer from cell matrix to the embedded MWCNTs under tensile force resulting from the strong interfacial interaction between MWCNTs and the polymer matrix, the latter agreed well with the conclusion from the cumulative pore volume calculation. Furthermore, the pullout effect of the incorporated MWCNTs in the composite fibers as seen in Figure 9 could also be helpful in improving the elongation of the MWCNT/cell composites as reported by others (10). Moreover, the improved diameter uniformity of the MWCNT/cell fibers could also contribute toward better mechanical properties (Figure 5). As observed earlier, only 30 to 40% of the fiber segments contained MWCNTs. The segments without MWCNTs would break first under tension, which could undermine the reinforcing effects by MWCNTs. Therefore, substantial improvement in tensile properties is likely by increasing MWCNT loadings in fibers and distributing the MWCTNs continuously along the lengths of the fibers.

CONCLUSIONS

MWCNTs were successfully incorporated into ultrafine cell fibers by electrospinning MWCNT loaded CA solutions, followed by aqueous alkaline hydrolysis to deacetylate CA to pure cell. The FTIR spectra and XRD patterns confirmed the deacetylation reaction and complete conversion from CA to cell. The presence of MWCNTs in the fibers was evident by SEM and TEM and verified by Raman spectra. With 0.11 and 0.55 wt % MWCNTs, the mean fiber diameter decreased from 267 nm for the pure cell to 237 and 193 nm, respectively, whereas the fiber sizes became more uniform. The MWCNT/cell fibrous sheets demonstrated remarkably fast as well as significantly improved equilibrium water wetting behavior as compared to pure cell. Moreover, the BET surface area also increased from 4.27 m^2/g of cell to 5.07 and 7.69 m^2/g of MWCNT/cell with ratios of 0.11 and 0.55 wt %, respectively. The fibers loaded 0.55 wt % MWCNT had doubled Young's modulus (553 to 1144 MPa) and tensile strength (21.9 to 40.7 MPa) while slightly increased elongation (from 8.04 to 10.46%). The significantly enhanced tensile properties at such low loading clearly reflect the well-aligned MWCNTs along the fiber axis observed by TEM. The fact that MWCNTs were observed in only a third of the fiber segments of the 0.55 wt % loaded fibers suggests further improvement of tensile properties to be easily achievable by increasing the MWCNT loading.

Acknowledgment. This research was made possible by funding from National Textile Center (project M02-CD05) as well as the Jastro-Shields Graduate Research Award and Summer Graduate Researcher Award from the University of California, Davis.

REFERENCES AND NOTES

(1) Iijima, S. *Nature* **1991**, *354*, 56–58.
(2) Treacy, M. M. J.; Ebbesen, T. W.; Gibson, J. M. *Nature* **1996**, *381*, 678–680.
(3) Wang, G.; Tan, Z.; Liu, X.; Chawda, S.; Koo, J.-S.; Samuilov, V.; Dudley, M. *Nanotechnology* **2006**, *17*, 5829–5835.
(4) Kang, J. W.; Song, K. O.; Kwon, O. K.; Hwang, H. J. *Nanotechnology* **2005**, *16*, 2670–2676.
(5) Kannan, P.; Eichhorn, S. J.; Young, R. J. *Nanotechnology* **2007**, *18*, 235707/1–235707/7.
(6) Chen, D.; Liu, T.; Zhou, X.; Tjiu, W. C.; Hou, H. *J. Phys. Chem. B* **2009**, *113*, 9741–9748.
(7) Naebe, M.; Lin, T.; Staiger, M. P.; Dai, L.; Wang, X. *Nanotechnology* **2008**, *19*, 305702/1–305702/8.
(8) Almecija, D.; Blond, D.; Sader, J. E.; Coleman, J. N.; Boland, J. J. *Carbon* **2009**, *47*, 2253–2258.
(9) Doshi, J.; Reneker, D. H. *J. Electrost.* **1995**, *35*, 151–60.
(10) Ye, H.; Lam, H.; Titchenal, N.; Gogotsi, Y.; Ko, F. *Appl. Phys. Lett.* **2004**, *85*, 1775–1777.
(11) Wan, L.-S.; Ke, B.-B.; Wu, J.; Xu, Z.-K. *J. Phys. Chem. C* **2007**, *111*, 14091–14097.
(12) Hou, H.; Ge, J. J.; Zeng, J.; Li, Q.; Reneker, D. H.; Greiner, A.; Cheng, S. Z. D. *Chem. Mater.* **2005**, *17*, 967–973.
(13) Ji, J.; Sui, G.; Yu, Y.; Liu, Y.; Lin, Y.; Du, Z.; Ryu, S.; Yang, X. *J. Phys. Chem. C* **2009**, *113*, 4779–4785.
(14) Ko, F.; Gogotsi, Y.; Ali, A.; Naguib, N.; Ye, H.; Yang, G.; Li, C.; Willis, P. *Adv. Mater.* **2003**, *15*, 1161–1165.
(15) Ge, J. J.; Hou, H.; Li, Q.; Graham, M. J.; Greiner, A.; Reneker, D. H.; Harris, F. W.; Cheng, S. Z. D. *J. Am. Chem. Soc.* **2004**, *126*, 15754–15761.
(16) Zhang, Q.; Chang, Z.; Zhu, M.; Mo, X.; Chen, D. *Nanotechnology* **2007**, *18*, 115611/1–115611/6.
(17) Huang, S.; Yee, W. A.; Tjiu, W. C.; Liu, Y.; Kotaki, M.; Boey, Y. C. F.; Ma, J.; Liu, T.; Lu, X. *Langmuir* **2008**, *24*, 13621–13626.
(18) Mazinani, S.; Ajji, A.; Dubois, C. *Polymer* **2009**, *50*, 3329–3342.
(19) Zhou, W.; Wu, Y.; Wei, F.; Luo, G.; Qian, W. *Polymer* **2005**, *46*, 12689–12695.
(20) Mei, F.; Zhong, J.; Yang, X.; Ouyang, X.; Zhang, S.; Hu, X.; Ma, Q.; Lu, J.; Ryu, S.; Deng, X. *Biomacromolecules* **2007**, *8*, 3729–3735.
(21) Kim, G. M.; Michler, G. H.; Poetschke, P. *Polymer* **2005**, *46*, 7346–7351.
(22) Hunley, M. T.; Poetschke, P.; Long, T. E. *Macromol. Rapid Commun.* **2009**, *30*, 2102–2106.
(23) Sundaray, B.; Subramanian, V.; Natarajan, T. S.; Krishnamurthy, K. *Appl. Phys. Lett.* **2006**, *88*, 143114/1–143114/3.
(24) Jose, M. V.; Steinert, B. W.; Thomas, V.; Dean, D. R.; Abdalla, M. A.; Price, G.; Janowski, G. M. *Polymer* **2007**, *48*, 1096–1104.
(25) Ayutsede, J.; Gandhi, M.; Sukigara, S.; Ye, H.; Hsu, C.-m.; Gogotsi, Y.; Ko, F. *Biomacromolecules* **2006**, *7*, 208–214.
(26) Feng, W.; Wu, Z.; Li, Y.; Feng, Y.; Yuan, X. *Nanotechnology* **2008**, *19*, 105707/1–105707/6.
(27) Schiffman, J. D.; Schauer, C. L. *Polym. Rev.* **2008**, *48*, 317–352.
(28) Esteves Magalhaes, W. L.; Cao, X.; Lucia, L. A. *Langmuir* **2009**, *25*, 13250–13257.
(29) Kim, C.-W.; Frey, M. W.; Marquez, M.; Joo, Y. L. *J. Polym. Sci., Part B: Polym. Phys.* **2005**, *43*, 1673–1683.
(30) Viswanathan, G.; Murugesan, S.; Pushparaj, V.; Nalamasu, O.; Ajayan, P. M.; Linhardt, R. J. *Biomacromolecules* **2006**, *7*, 415–418.
(31) Frey, M. W.; Joo, Y. L. Cellulose solution in solvent and electrospinning thereof. Patent 2004834041 2005247236, 20040429, 2005.
(32) Frey, M. W. *Polym. Rev.* **2008**, *48*, 378–391.
(33) Kim, C.-W.; Kim, D.-S.; Kang, S.-Y.; Marquez, M.; Joo, Y. L. *Polymer* **2006**, *47*, 5097–5107.
(34) Liu, H.; Hsieh, Y.-L. *J. Polym. Sci., Part B: Polym. Phys.* **2002**, *40*, 2119–2129.

(35) Shukla, S.; Brinley, E.; Cho, H. J.; Seal, S. *Polymer* **2005**, *46*, 12130–12145.
(36) Frenot, A.; Henriksson, M. W.; Walkenstroem, P. *J. Appl. Polym. Sci.* **2007**, *103*, 1473–1482.
(37) Godinho, M. H.; Canejo, J. P.; Pinto, L. F. V.; Borges, J. P.; Teixeira, P. I. C. *Soft Matter* **2009**, *5*, 2772–2776.
(38) Lu, P.; Hsieh, Y.-L. *J. Membr. Sci.* **2009**, *330*, 288–296.
(39) Hsieh, Y.-L. *Text. Res. J.* **1995**, *65*, 299–307.
(40) Lu, P.; Hsieh, Y.-L. *J. Membr. Sci.* **2009**, *348*, 21–27.
(41) Lu, P.; Hsieh, Y.-L. *Carbohydr. Polym.* **2010**, *82*, 329–336.
(42) Dinand, E.; Vignon, M.; Chanzy, H.; Heux, L. *Cellulose* **2002**, *9*, 7–18.
(43) Dror, Y.; Salalha, W.; Khalfin, R. L.; Cohen, Y.; Yarin, A. L.; Zussman, E. *Langmuir* **2003**, *19*, 7012–7020.
(44) Salalha, W.; Dror, Y.; Khalfin Rafail, L.; Cohen, Y.; Yarin Alexander, L.; Zussman, E. *Langmuir* **2004**, *20*, 9852–5.

AM1004128